Polymer-based 3D printing of function-integrated optomechanics – design guidelines and system evaluation

Fabian Kranert and Moritz Hinkelmann
Laser Zentrum Hannover e.V., Hannover, Niedersachsen, Germany and
Cluster of Excellence PhoenixD (Photonics, Optics, and Engineering – Innovation Across Disciplines), Hannover, Germany
Roland Lachmayer
Laser Zentrum Hannover e.V., Hannover, Niedersachsen, Germany;
Cluster of Excellence PhoenixD (Photonics, Optics, and Engineering – Innovation Across Disciplines), Hannover, Germany and
Institut für Produktentwicklung und Gerätebau, Leibniz Universität Hannover, Garbsen, Germany, and
Jörg Neumann and Dietmar Kracht
Laser Zentrum Hannover e.V., Hannover, Niedersachsen, Germany and
Cluster of Excellence PhoenixD (Photonics, Optics, and Engineering – Innovation Across Disciplines), Hannover, Germany

Abstract

Purpose – This study aims to extend the known design guidelines for the polymer-based fused filament fabrication (FFF) 3D printing process with the focus on function-integrated components, specifically optomechanical parts. The potential of this approach is demonstrated by manufacturing function-integrated optomechanics for a low-power solid-state laser system.

Design/methodology/approach – For the production of function-integrated additively manufactured optomechanics using the FFF process, essential components and subsystems have been identified for which no design guidelines are available. This includes guidelines for integrating elements, particularly optics, into a polymer structure as well as guidelines for printing functional threads and ball joints. Based on these results, combined with prior research, a function-integrated low-power solid-state laser optomechanic was fabricated via the FFF process, using a commercial 3D printer of the type Ultimaker 3. The laser system's performance was assessed and compared to a reference system that employed commercial optomechanics, additionally confirming the design guidelines derived from the study.

Findings – Based on the design goal of function integration, the existing design guidelines for the FFF process are systematically extended. This success is demonstrated by the fabrication of an integrated optomechanic for a solid-state laser system.

Practical implications – Based on these results, scientists and engineers will be able to use the FFF process more extensively and benefit from the possibilities of function-integrated manufacturing.

Originality/value – Extensive research has been published on additive manufacturing of optomechanics. However, this research often emphasizes only cost reduction and short-term availability of components by reprinting existing parts. This paper aims to explore the capabilities of additive manufacturing in the production of function-integrated components to reduce the number of individual parts required, thereby decreasing the workload for system assembly and leading to an innovative production process for optical systems. Consequently, where needed, it provides new design guidelines or extends existing ones and verifies them by means of test series.

Keywords Fused filament fabrication, 3D printing, Additive manufacturing, Design guidelines, 3D printed optomechanics

Paper type Research paper

1. Introduction

In recent years, additive manufacturing (AM) has been established as a complementary manufacturing method in both research and industry (Gibson *et al.*, 2015; Jordan, 2018). In addition to the well-known benefits of increased design freedom, as well as material and weight savings, AM allows for the production of function-integrated

The current issue and full text archive of this journal is available on Emerald Insight at: **https://www.emerald.com/insight/1355-2546.htm**

Rapid Prototyping Journal
30/11 (2024) 247–259
Emerald Publishing Limited [ISSN 1355-2546]
[DOI 10.1108/RPJ-02-2023-0073]

This research was funded within the framework of the project "GROTESK - Generative Fertigung optischer, thermaler und struktureller Komponenten" by EFRE - NBank (ZW6-85017815) and under Germany's Excellence Strategy within the Cluster of Excellence PhoenixD (EXC, 2122, Project ID 390833453) by the Deutsche Forschungsgemeinschaft (DFG, German Research Foundation).

Received 28 February 2023
Revised 13 September 2023
9 January 2024
22 April 2024
Accepted 14 May 2024

components, i.e. the implementation of several technical features in a single part, thereby reducing the number of discrete components (Yang and Zhao, 2015). Thus, it is an enabling technology for digitized production in the context of Industry 4.0 (Dilberoglu, *et al.*, 2017; Haleem and Javaid, 2019). Currently, a wide range of additive manufacturing processes can be applied to a variety of materials, from polymers and metals to glasses and ceramics (Calignano, *et al.*, 2017). Fused filament fabrication (FFF), among others, is a mature and widely used method for polymer printing. A thermoplastic polymer material is conveyed in the form of a filament into a heated nozzle and extruded from it onto a build platform. By placing lines next to each other, a two-dimensional structure is created, and by lowering the platform stepwise and stacking multiple layers on top of each other, a three-dimensional object is generated. In addition to its ease of use, the process is characterized by low prices for machines and materials, making it interesting for end-user applications, especially in the field of research and education (Pearce, 2012). Additionally, the FFF process offers two manufacturing possibilities that make it particularly interesting for the production of function-integrated components. These are multimaterial printing (Espalin, *et al.*, 2014), i.e. the use of two or more materials in a single print job, and the imprinting of components directly into the polymer matrix, which is described as the print-pause-print (PpP) process (Pinger, *et al.*, 2017; Li, *et al.*, 2019).

A field in research, where FFF is widely used owing to its cost-effective and easy-to-use technology, is the 3D printing of optomechanical components. A variety of applications have already been demonstrated which exploit 3D printing for manufacturing components used in the alignment and mounting of discrete optical elements as well as their use in various laboratory setups (Salazar-Serrano, *et al.*, 2017; Zhang, *et al.*, 2013). These setups include interferometry, bright-field microscopy, and spectrophotometry for measurement applications (Davis, *et al.*, 2018; Gunderson, *et al.*, 2020; Winter and Shepler, 2018). Thereby, commercially available parts are mostly reprinted without any further consideration on the design or function integration. The first approaches to take the advantages of AM into account are adaptable but structure-bounded kits, where different attachments, such as holders for lenses, light sources, or cameras, can be mounted on a base body (Delmans and Haseloff, 2018; Diederich *et al.*, 2020). Even higher integrated systems for special tasks, like microscopy (Maia Chagas, *et al.*, 2017; Nuñez, *et al.*, 2017), different kinds of spectrometry (Aydogan and Tasal, 2018; Pereira and Hosker, 2019; Porter *et al.*, 2016) and optical characterization (Zou, *et al.*, 2016; Nadal-Serrano *et al.*, 2017), have been demonstrated. Common to all these systems is that they have been developed with the goal of keeping costs as low as possible and ensuring short-term availability through on-site production, with little effort to use AM for more compact systems and the integration of discrete elements into a combined assembly. In contrast, this paper exploits the potential of the FFF process to highlight the opportunities for the fabrication of function-integrated optomechanical assemblies. Therefore, the traditional optomechanical design based on discrete elements must be reevaluated. Accordingly, a suitable product development process should be selected. The V-model (VDI/VDE-Gesellschaft Mess- und Automatisierungstechnik, 2021), which was originally created for the development of cyber-physical systems, can be applied for this purpose. To mark the high potential, the sophisticated optomechanical setup of a diode-pumped solid-state laser (DPSSL) is chosen as a representative optical system, which sets demanding requirements in terms of structural and thermal properties to enable stable laser operation. While previous research has already demonstrated the fundamental feasibility of such a system (Kranert *et al.*, 2022), the focus of this study is to derive design guidelines for elements that have proven to be necessary for function-integrated manufacturing based on the DPSSL. The guidelines, validated in the specific case study of the DPSSL, are formulated in a generalized manner to facilitate transfer to other applications where function integration is required.

2. Design guidelines

The design of components is always determined by design objectives and restrictions imposed by the manufacturing process, whereby the needs of users and the market must also be considered (Kerbrat *et al.*, 2011). Design guidelines should support the user in this development process. The guidelines should be universally applicable and independent of the final product (Mani *et al.*, 2017). To ensure effective implementation, the knowledge and experience gained must be generalized into applicable guidelines. AM processes have required the development of new design guidelines, as these processes enable different component designs, but also have their own restrictions (Diegel, 2022). This helps the designer comply with the constraints of AM processes when creating components. The guidelines ensure that the desired component can be manufactured, fulfills its functionality, and can be produced cost-effectively (Medellin-Castillo and Zaragoza-Siqueiros, 2019). Design guidelines are essential to fully realize the potential of additive AM and have been crucial to the widespread adoption of the AM technology in the industrial sector (Thompson, *et al.*, 2016) and are the basis for the production of end-use parts (Adam and Zimmer, 2014). Design guidelines for AM incorporate various aspects such as component accuracy, the use of support structures, surface quality, component size limitations, and minimum wall thicknesses (Gibson *et al.*, 2015; Ko *et al.*, 2015). Depending on the specific AM process, these guidelines must be extended to include machine- and material-specific constraints to ensure the quality and reproducibility of the parts produced. Design guidelines may sometimes conflict with each other, and the designer must prioritize them based on the application. Some researchers attempted to establish design guidelines that are generally applicable to various AM processes, e.g. Fused deposition modeling, laser sintering and laser melting (today referred to as laser beam powder bed fusion) (Adam and Zimmer, 2014; Adam and Zimmer, 2015).

Regarding the FFF process, specific design guidelines can be established to systematically consider its peculiarities, such as the use of thermoplastic materials and the presentation of the material as a filament. Guidelines for this process are crucial since the FFF process is widely used in the industrial, academic and private sector, where they are needed as guidance for inexperienced users through the design process (Djokikj and Kandikjan, 2022). There are numerous studies on the FFF process, each addressing different aspects. An overview can be found by Pradel *et al.* ((2018). General guidelines for designing for FFF are presented in Urbanic and Hedrick (2016) and Steuben *et al.* (2015), as well as specific guidelines for rapid tooling. Alafaghani *et al.* ((2017) offer an

extensive review of the design considerations to enhance part quality, supplemented by their own research. Medellin-Castillo and Zaragoza-Siqueiros (2019) also provide a list of general design guidelines and extend them with mathematical models to calculate the part cost and energy consumption. All of the aforementioned works include case studies to validate their findings. Djokikj and Kandikjan (2022) supplement general guidelines with precise numerical values for designing print features based on given print parameters. These guidelines specify minimum wall thicknesses, maximum bridge widths, and minimum distances between stand-alone features, among other specifications. The information serves as a foundation for producing parts successfully through this process.

3. Methods

As previously mentioned, the V-model (VDI/VDE-Gesellschaft Mess-und Automatisierungstechnik, 2021) is used for the development of a functionally integrated optomechanical system. The original model evolved in various forms based on the experience gained (Gräßler, *et al.*, 2018). In the following, the so-called 3-level model is applied, which is divided into system, subsystem, and component levels (cf. Figure 1). The V-model begins with requirement elicitation, which defines the system's capabilities to be achieved. The measurement methods must be planned in this step to verify the fulfillment of these requirements. Based on this, a system design for the product is created at the system level, in which the main functions and dependencies are considered. The system is decomposed into subsystems occurs along the left leg of the V. Here, the defined functions are detailed, followed on the component level by the actual realization of the system elements, which are derived from the subsystems. The developed and verified components are then integrated along the right leg of the V into the subsystems, which are tested against the defined requirements. This ensures that problems are identified and solved through an iterative optimization process, continuously increasing the quality of the overall solution (Wynn, *et al.*, 2010). The final verification occurs after the subsystems have been integrated into the complete system. When applying this model to the development of the DPSSL, the requirements can be divided into three areas. The first summarizes the constraints provided by the 3D printer

Figure 1 V-Model in the 3-level approach for the development of optomechanical systems

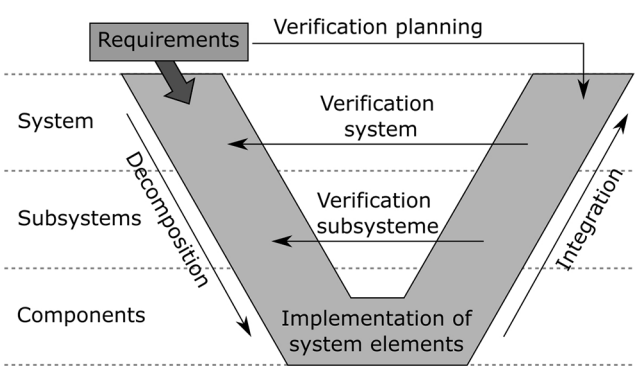

Source: Kranert, (2024)

Ultimaker 3 from *Ultimaker*, which limits the size of the system by its building space and usable materials. The second area deals with the requirements for the design of optomechanics and describes the conditions to enable functional and efficient printing. This was achieved by adhering to prescribed design principles outlined in the above section, which establish guidelines for the minimum wall thickness and angles for overhangs that do not require support structures. This ensures that the basic design of the optomechanic meets the manufacturing requirements of the FFF process. The third category addresses the requirements of the manufactured solid-state laser system. The core requirement is stable laser operation using printed optomechanics. Furthermore, it is intended to achieve output power and efficiency characteristics similar to those of a comparable system based on commercially available discrete optomechanics. This proves that high demands, especially in terms of the optical resonator's stability, can be met. To verify the system against its requirements, a comprehensive analysis and evaluation of the final laser system is performed, including a series of tests, e.g. to determine the long-term behavior. All assessed parameters and their measurement procedures are presented in Section 5, accompanied by the corresponding results. Decomposing the laser system along the V-model reveals three elements that are of specific importance regarding the system's implementation. Each of these elements has constituent parts that require a design solution for implementation under the goal of function integration, which the current design guidelines do not address. (1) At the component level, fixing the optical elements to specific positions in the optomechanical system is necessary. This is required to transfer a simulated optical design into real optomechanics and to enable laser operation. Thus, a suitable design for integration into the polymer matrix via the PpP process is requested, without inducing additional mechanical stress, while at the same time providing the required level of accuracy and stability for laser operation. (2) At the subsystem level, this concerns the heat sink of the laser crystal, which is essential for both holding and cooling this component to enable efficient laser operation (Délen, *et al.*, 2011). To achieve this objective, waterproof threads should be utilized for the cooling water connection as they facilitate better integration with functional components, negating the need for extra connection components. (3) Also at the subsystem level, optomechanical devices that can be adjusted must be included to manipulate the resonator mirrors. This will enable optimal overlap of the pump and resonator transverse modes, which is essential for the efficiency of the lasing process and the stability of the output power over time (Koechner, 2006). Therefore, ball joints are necessary to align in two axes. By printing them, like the threads, the function integration of the system increases. Figure 2 provides a graphical summary of these points. The design rules for the DPSSL optomechanical system are implemented along the right leg of the V-model. The verification of their functionality is achieved through testing the laser system. Although the necessity for these elements originates from a specific application, it is evident that they can enhance the potential of the FFF process by broadening its applicability to different application areas. For this purpose, generally applicable guidelines are derived from those specific to this application, thus supplementing those given in literature.

Figure 2 V-model for a function-integrated laser system with the relevant development steps derived

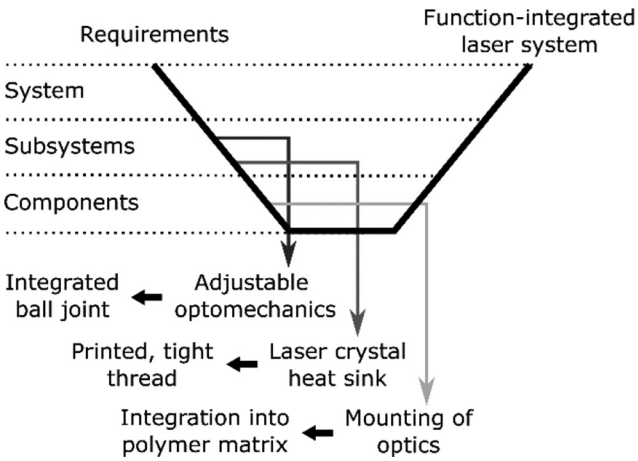

4. Design guidelines

As described, three constituent parts have been identified for which design guidelines should be available to enable the FFF-based production of function-integrated systems. It is essential to identify an appropriate sample design for each case. Additionally, it is necessary to define printing parameters for manufacturing and to evaluate the produced test samples. The evaluation results allow the actual design guidelines to be formulated. The function-integrated laser system case study validates them.

As stated in Section 1, function integration can also be promoted using multi-material printing. Therefore, two distinct materials were chosen depending on the intended application in the system. The first material is an inexpensive, standard polylactate (PLA), while the second material is a composite PLA material containing copper particles (Cu-PLA). The second one was examined due to its higher thermal conductivity (Elkholy, *et al.*, 2019). This makes it advantageous for producing heat sinks, such as those used in laser crystals (Kranert *et al.*, 2021a, Kranert *et al.*,2021b; Röttger *et al.*, 2021). The printing parameters are listed in Table 1.

4.1 Integration of optical elements into a polymer matrix

The importance of placing the discrete optical elements in a defined position along the optical axis within the integrated optomechanics has already been described. Optics in laboratory setups are typically fastened with a side-engaging screw, pressing them against the frame, or with a retaining ring engaging the optical surface (Yoder, 2008). For integrated optomechanics, additional fixation components, such as screws, should be avoided. It has already been shown that the PpP scheme offers the potential to imprint an optical element directly at its respective position in an optomechanical system (Kranert *et al.*, 2022). Figure 3 shows the corresponding steps, of the PpP-scheme. In the construction file, a decisive recess for the optic must be provided. The optical element is inserted during a pause in the printing process and fixed in place by the polymer material overlapping the optics after printing is resumed. The following discussion is limited to optical elements with cylindrical geometry, as this is usually the case for lenses and mirrors. The applicable diameters are 12.7 mm (½") and 25.4 mm (1"). The evaluation of the sample design is based on specific criteria such as proper insertion of the optic into the recess and secure fixation after imprinting with minimal mechanical stress. To fit an optic into the circular recess, the appropriate diameter d must be determined (cf. Figure 4(a)). Using the same size as the optical element is not feasible as the limited accuracy of the FFF process (Gibson, *et al.*, 2015) results in the recess being too small. Therefore, the diameter must be larger than that of the component to be inserted. By gradually increasing the diameter, it was found that, for both the 12.7 mm (½") and 25.4 mm (1") optics, the diameter of the cutout should be 0.4 mm wider. While this is sufficient for most structural elements, applying this procedure to optics will cause mechanical stress, which is induced by the z-seam created during the printing process (Gibson, *et al.*, 2015) and potentially leading to depolarization losses, i.e. a lower laser efficiency. Increasing the allowance of the diameter to compensate for the z-seam is not effective because a tight fit of the optic in the x-y-plane is no longer guaranteed. For this reason, as shown in Figure 4(a), an undercut was added to the round recess to allow the seam to be formed at the tip of the undercut (Gibson, *et al.*, 2015). Thereby, the issue with the z-seam is resolved, but bulges are generated at the transition from the recess to the undercut. This occurs because the print head must substantially change direction of movement when transitioning from the circular path of the recess to the tip of the undercut, resulting in over-extrusion of material at that point. An introduction of mechanical stress is once again caused by the bulges. Therefore, extra roundings were included at the transition of the recess to the undercut. Measurements of the induced mechanical stresses showed that a radius of $r = 3$ mm should be selected. Thus far, only the requirements for the shape of the recess have been discussed. However, for the fixation of elements in the polymer matrix, the depth of the recess and the width of the fixing lands must be considered. The depth of the recess h (cf. Figure 4(b)) must be designed to be smaller than the height of the inserted element to ensure a form-fit connection. Accordingly, a height difference between this element and the

Table 1 Slicing software and most important printing parameters for the two different materials used

Parameter	PLA	Cu-PLA
Slicing software	Ultimaker Cura 4.4	
Layer height / mm	0.2	0.2
Nozzle diameter / mm	0.4	0.6
Infill / %	20	100
Flow / %	100	130
Shell thickness / mm	1.0	1.3
Printing temperature / °C	205	200
Platform temperature / °C	60	60

Source: Table by authors

Figure 3 PpP scheme for embedding an optic in a 3D printed optomechanics

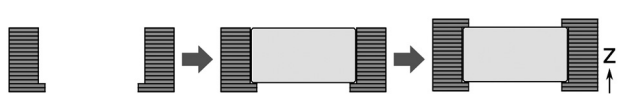

Source: Kranert, (2024)

Figure 4 Relevant parameters for the design constraints for low-stress mounting of round optical elements

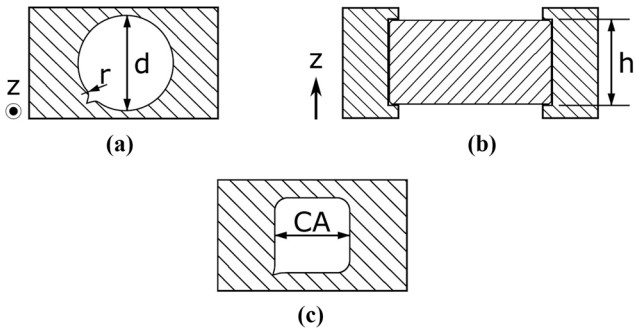

Notes: (a) Top view; (b) cross section through optomechanics with imprinted optic; (c) top view after the imprinting
Source: Kranert, (2024)

surrounding polymer matrix of one layer thickness or less must be selected to prevent the nozzle from hitting the element. Furthermore, path guidance for the layers fixating the element must be considered. Stable adhesion is achieved only when printing onto an underlying polymer layer. For this reason, imprinting should be achieved using straight lines passing over the element and not concentric ones (cf. Figure 4(c)). The width of the generated lands should be as narrow as possible to avoid warping effects, i.e. the bending of the printed contours from the inserted, cold element to the hot nozzle, and to allow for the largest possible clear aperture (CA). Land widths of 1.5 mm for ½" optics and 2.5 mm for 1" optics are found to be suitable.

In the scenario depicted in Figure 4, the imprinted component has two flat surfaces. Certain components like lenses exhibit a curved surface instead. Accordingly, two additional cases must be considered depending on the direction of the curved surface with respect to the printing direction (cf. Figure 5). In the first case, the flat side of the lens faces up, allowing the lands to be printed over this surface. Only the bottom of the recess must be adjusted according to the lens curvature. In the opposite case, the curved side of the lens is oriented upward, such that the print head would collide with the lens. Accordingly, a suitable adapter must be used, which

Figure 5 Integration of a plano-convex lens using the PpP-scheme

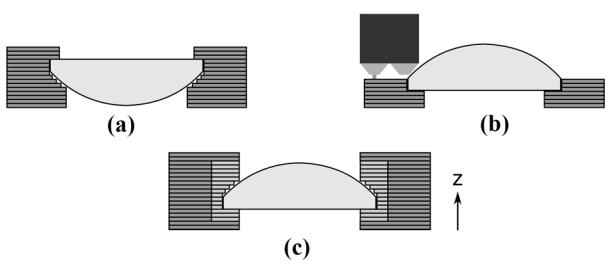

Notes: (a) The convex side points downward; (b) convex side points upwards and collides with the print head; (c) the lens is imprinted in an adapter and then this adapter is imprinted in the actual optomechanics
Source: Kranert, (2024)

fixates the lens and simultaneously provides a flat surface for imprinting in the final structure. This leads to the necessity of an additional process step. Therefore, the adapter can be a commercial solution or an upstream printed part in which the component is integrated, as in the first case. While only qualitative statements have been made for the development of the design guidelines, this will be validated quantitatively in the following. Figure 6 shows the results of the stress measurements of an N-BK7 lens (LA1509-B; Thorlabs, Inc.) with a diameter of 1". Measurements were performed using a polarimeter. For imprinting, only PLA was considered. The lens was imprinted with the flat side facing upward, and the curvature on the contact surface for the lens in the printed optomechanic (cf. Figure 5(a)) corresponds to the radius of curvature of the lens of 51.5 mm. Five cases were examined, including the three development steps during the investigation of the design guidelines:

1 the lens is not mounted, which means that it lies in a commercial mount but is not fixated.
2 The lens is fixated in a commercial mount using a retaining ring.
3 The lens is imprinted using the PpP scheme without an undercut.
4 The lens is imprinted using the PpP scheme with an undercut, but without rounding.
5 The lens is imprinted using the PpP scheme with an undercut with a rounding radius of 3 mm.

The bars that fix the optics in place during imprinting cause the recognizable rectangular aperture (cf. Figure 4(c)), whereas the commercial holder produces a round aperture. Table 2 lists the measured average and maximum mechanical stresses for the different cases. The design with the undercut but without rounding exhibited the highest stress values. Stress occurs in the lower right corner of the corresponding graph (Figure 6(d)) caused by the bulges appearing at the transition between the round recess and the undercut. The commercial mount and the simple recess without design optimization also lead to an increased maximum stress inside the optic, although less pronounced with only half the stress value. The commercial mount exhibited the highest average stress. For the final design of the additive optomechanics, the measurement yields the same maximum stress value of 0.34 MPa as in the unmounted case. Thus, the results show, on the one hand, that the stress-free support by the PpP scheme is possible and, on the other hand, how important the appropriate design of the 3D printed part is and, hence, the importance of the derived design guidelines.

4.2 Printed threads

Initial results for the FFF printing of internal threads have already been documented in the literature with respect to their use in flow chemistry (Price *et al.*, 2021) and selected metric threads (Farniev *et al.*, 2022; Nefelov and Baurova, 2017). To scale the potential of function integration, the following investigations will cover the use of threads in combination with different screw diameters, but also their applicability to water connections in the heat sink of a laser crystal, since this is the specific use case in DPSSL. The test sample used is shown in Figure 7. The prints were based on the printing parameters listed in Table 1 and both materials, PLA and Cu-PLA, are considered. The design feature

Figure 6 Mechanical stress in a N-BK7 lens mounted in different optomechanics. The false color scale is valid for all diagrams

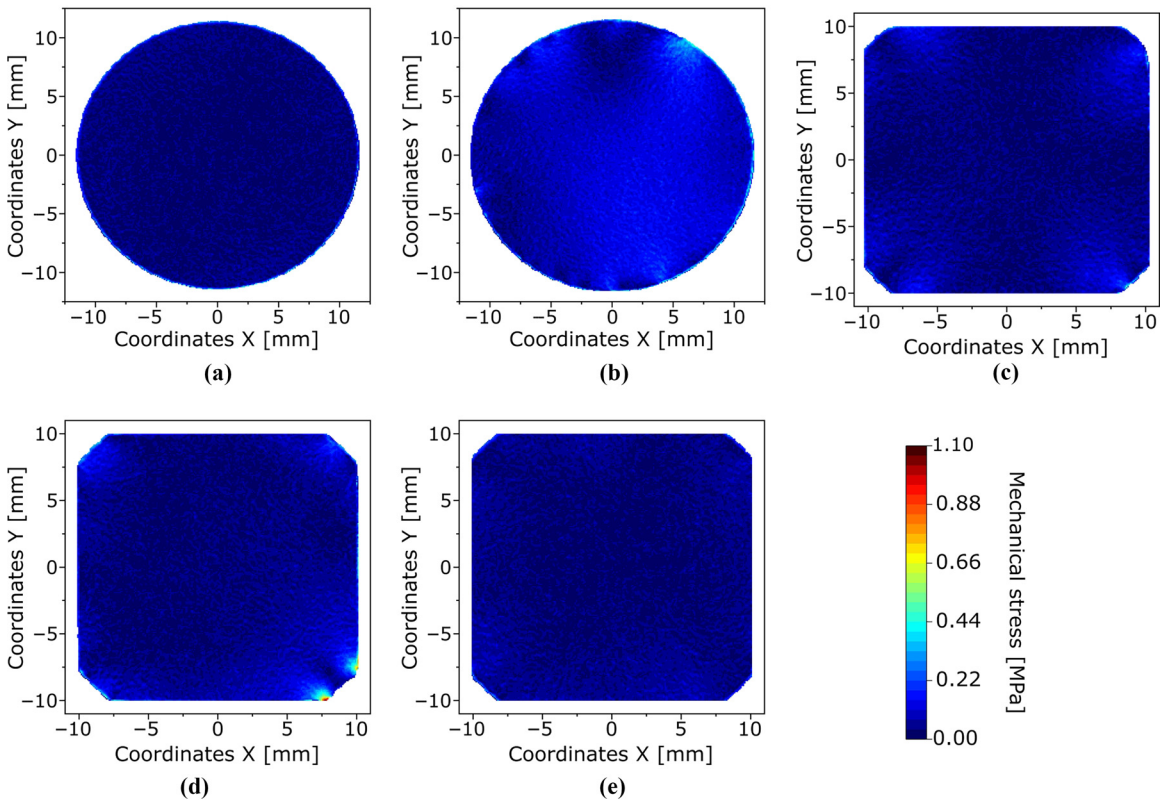

Notes: (a) The lens is not mounted; (b) the lens is mounted in a commercial mount with a retaining ring; (c) the lens is imprinted using the PpP scheme without an undercut; (d) the lens is imprinted using the PpP scheme with an undercut but without a rounding; (e) the lens is imprinted using the PpP scheme with an undercut with a rounding radius of 3 mm
Source: Kranert, (2024)

Table 2 Listing of the average and maximum mechanical stress within a glass lens for different methods of mounting and different designs of additively manufactured holders

Mounting	Mean mech. Stress / MPa	Max. mech. Stress / MPa
Unmounted	0.05	0.34
Fixed with retainer ring	0.11	0.48
Imprinted without undercut	0.08	0.52
Imprinted with undercut and without fillet	0.08	1.04
Imprinted with undercut and fillet with 3 mm radius	0.08	0.34

Source: Kranert, 2024

to be investigated is the core hole diameter d_c. The goal is to determine the appropriate size selection required to achieve a functioning thread. The tested core hole diameters are listed in Table 3. Thread sizes M3, M4, M5, M6 and G1/8" were examined. For both materials, each core hole diameter was printed four times. The general requirement for printing threads is that they are aligned along the printing direction, as shown in Figure 7.

Figure 7 Relevant parameters and orientation for the 3D printed thread

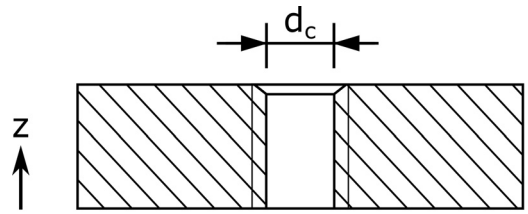

Source: Kranert, (2024)

When a thread is horizontally oriented, it gets distorted while being printed. The tested threads had a length of 5 mm, equivalent to the height of the entire test sample, and an additional 45° x 0.5 mm chamfer at the beginning. This facilitates insertion of the screw into the thread. The starting point for the diameters was the corresponding norm DIN 336 (DIN336, 2003). As expected, these diameters are too small, and larger ones must be selected to reach the desired results. Comparing the two materials, it can be seen that larger diameters are required for Cu-PLA than for PLA. This can be explained by the larger nozzle diameter of 600 μm used for Cu-PLA and the related reduced resolution. Based on

Table 3 Tested diameters for the core holes of printed threads

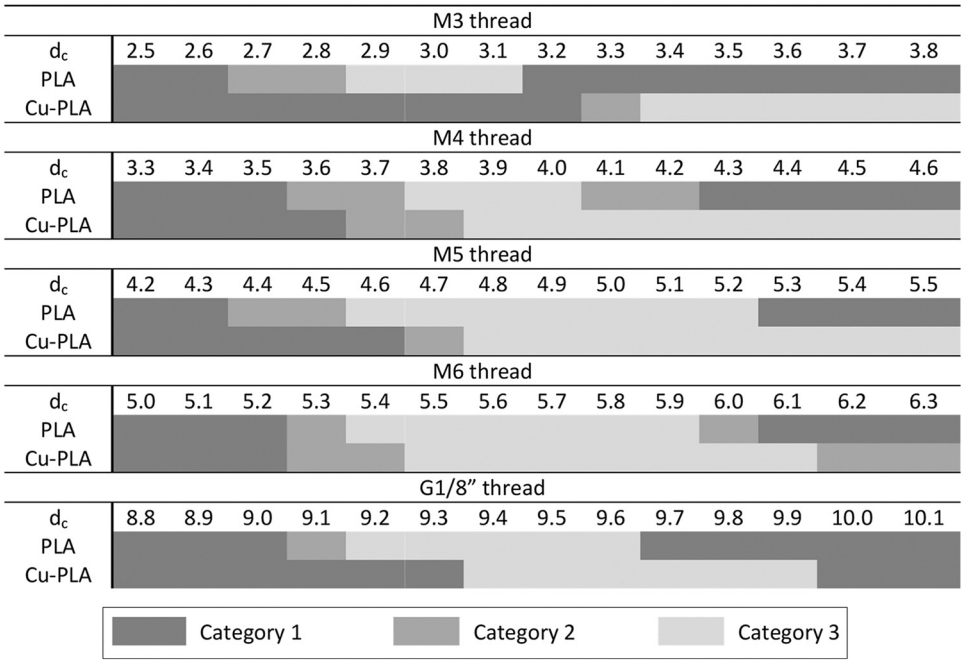

Notes: The quality was evaluated in three categories. In Category 1, it is not possible to drive in a screw since the thread is too large or small, respectively. In Category 2, the screw can only be driven in with great effort or is loose afterwards. In Category 3, the screw has the desired fit. The investigation was carried out for PLA and Cu-PLA material
Source: Kranert, 2024

these results, a further series of tests was conducted to determine the core hole design parameter for which a M5 and G1/8" threads were leak-free after water connectors were screwed into the printed threads. Therefore, the design in Figure 7 was expanded. Its height was increased to 20 mm so that a thread could be printed on each side of the channels with different diameters. Each thread exhibits a depth of 4 mm. An appropriate water connection is installed on both sides of the channel, connected to a water pump, and the connection is checked for leakage. The results are presented in Table 4. It is clear that the acceptance field is significantly narrower than when screws are used. In particular, for the combination of a G1/8" thread and Cu-PLA material, only one functional core hole diameter could be found. Nevertheless, the test sample proves that it is possible to produce printed threads that are leak-free.

4.3 Printed ball joint

The optical resonator of the laser system demands adjustable mirror mounts to enable the alignment of the pump light and laser mode to each other. Previous work has already demonstrated the functionality of printed adjustable optomechanics (Kranert *et al.*, 2021a, Kranert *et al.*, 2021b). The CAD models of the mounts are shown in Figure 8. It is evident, that this part cannot be printed without additional support structures for the spring system and ball socket, which necessitates removal in a post-processing step. The examined design guidelines focus on the ball joint itself and the requirements for producing it in a single print. The basis for the determination follows the design recommendation for the gap dimensions in the VDI guideline VDI 3405 Sheet 3.4 (VDI-Fachbereich Produktionstechnik und Verfahrenstechnik, 2021).

Table 4 Tested diameters for the core holes of printed threads used for water connection

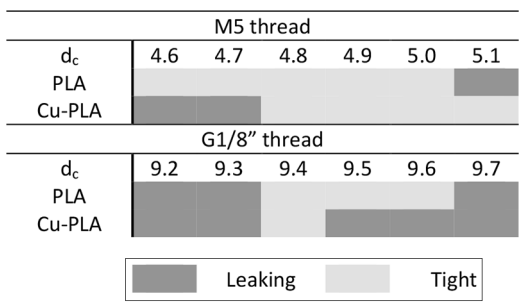

Note: The quality was evaluated according to whether water leaks or not. The test was carried out for PLA and Cu-PLA material
Source: Kranert, 2024

Unlike the case presented there, round surfaces are involved, so a new test sample was designed to determine the required distance *b* (cf. Figure 9(a)) between the ball and the socket to print a freely movable joint. Simultaneously, the clearance between the two elements should be kept as small as possible. The tests were carried out with PLA and the printing parameters listed in Table 1, but a higher print resolution was achieved by setting the layer height to 100 μm. As shown in Table 5, gap sizes in the range of 200 – 290 μm were investigated. Therefore, the ball joint was gradually reduced in size in the test samples, which resulted in a

Figure 8 (a, b) Printed, adjustable mirror mount with imprinted 1/2″ inch mirror; (c) mirror mount (1) imprinted into frame (2) with integrated fine thread screw. The arrows depict the printing direction

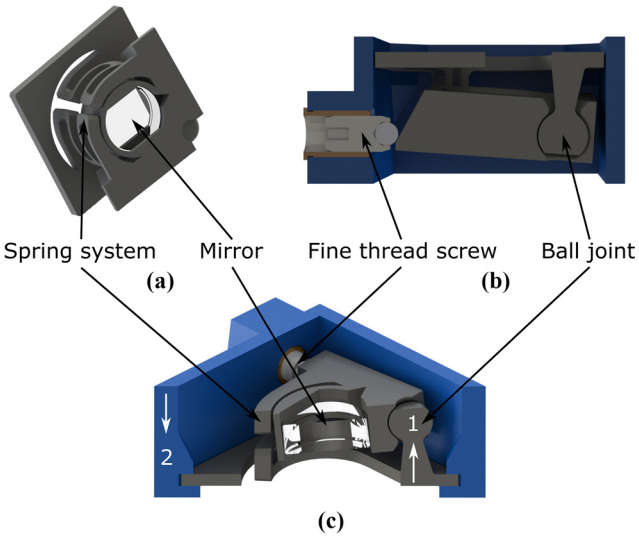

Source: Kranert, (2024)

stepwise increase in the gap dimension. Support structures were utilized to print the socket element in the test samples. Five specimens were manufactured for each gap size. For the evaluation, three categories are defined. Category 1 consists of joints that cannot be moved even when force is applied. Category 2 includes joints that stick to the socket but can be moved after force is applied. Category 3 comprises joints that can be moved immediately after printing. The results indicate that a gap size of 250 μm in the design reliably provides a functional joint. An increase in gap size affects the stability of the joint, potentially leading to negative long-term behavior or increased crosstalk between the two axes. Therefore, it is not recommended to use gaps larger than 250 μm.

4.4 Derived guidelines

Table 6 presents the guidelines derived from the above research for the identified constituent parts. For better clarity, general and special guidelines are combined. The specific numerical guidelines are only valid when using the designated printing settings. They still offer useful guidance for users even when other parameters are employed.

Figure 9 (a) Drawing of cross section through ball joint; (b) CAD model of the test specimen

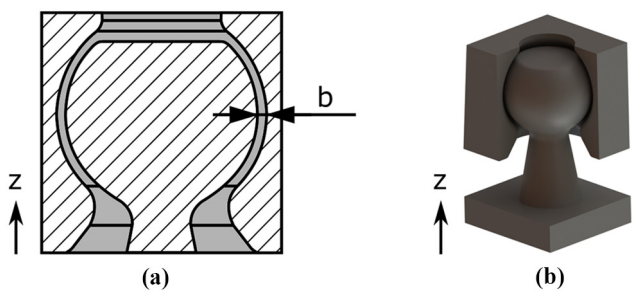

Source: Kranert, (2024)

Table 5 Determination of the required gap size in the ball joint, to allow free movement after printing

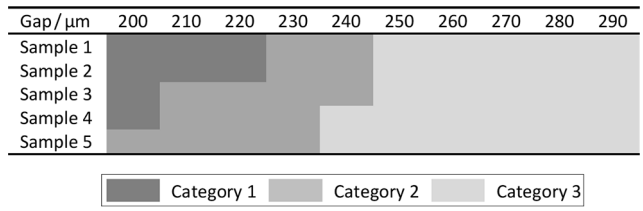

Notes: The prints are classified in three categories. In Category 1, the joint cannot be moved even with the use of force. In Category 2, the joint can be moved after breaking the socket free by force and in the last Category 3, the joint can already be moved freely after printing
Source: Kranert, 2024

5. Function-integrated laser system

5.1 Laser system design

As previously stated, the design guidelines developed will be verified through the case study of the DPSSL. The focus is to convert a traditional laboratory setup using discrete optomechanics (various components; Thorlabs, Inc.) into a laser system with function-integrated optomechanics (cf. Figure 10). The design

Table 6 Overview of design guidelines for the different constituent parts derived from experiments

Constituent part	Design guidelines
Integration of elements into polymer matrix	Recess diameter is 0.4 mm wider tHan tde element Undercut in design to conceal interfering z-seam Recess depth is one layer height smaller than the element height Lands for fixating an element should be narrow to avoid warping effects. Suitable for 1/2″ elements are 1.5 mm and 2.5 mm for 1″ elements To ensure stable adhesion, printing of the lands should begin on the surrounding polymer instead of the inserted element The imprinting of elements requires a flat surface, or suitable adapters should be used
Printed thread	Thread is orientated perpendicular to the printing direction Including a 45° x 0.5 mm chamfer at the beginning of the thread enhances the insertion of the screw Larger nozzle diameter requires for larger core hole diameter Suitable core hole diameters for different thread dimensions are given in Tables 3 and 4
Printed ball joint	Recommended gap between ball and socket is 250 μm to prevent them from sticking together Wider gaps increase the ball play in the socket

Source: Table by authors

guidelines developed will be utilized for this transfer. Therefore, the characterization of the laser system will validate their applicability. Figure 10(a) shows in the upper part a sectional view in the CAD-model of the 3D printed optomechanic in which the components are implemented during printing using the PpP scheme. The corresponding cutouts for these components are designed in accordance with the investigated guidelines outlined in Section 4.1. The described usage of multi-material printing optimizes the optomechanics to meet the requirements of laser operation and efficient, i.e. cost and weight effective, printing. Accordingly, the majority of the optomechanic - colored blue - is made from inexpensive and light PLA material. Cu-PLA was used only for the heat sink, in which the laser crystal was placed. The heat sink is designed with two threads to integrate the cooling water connectors (cf. Section 4.2.). The lower part of Figure 10(a) depicts the view with the imprinted optics and optomechanics, such as the adjustable mirror mounts with ball joints from Section 4.3 (gray). These have been printed separately due to the need for support structures.

Figure 10 (a) Cross section of the laser system. Top: Only the to be printed optomechanic. Bottom: The optomechanic with all needed mechanical and optical components. (b) Model of the corresponding reference system based on conventional optomechanics.

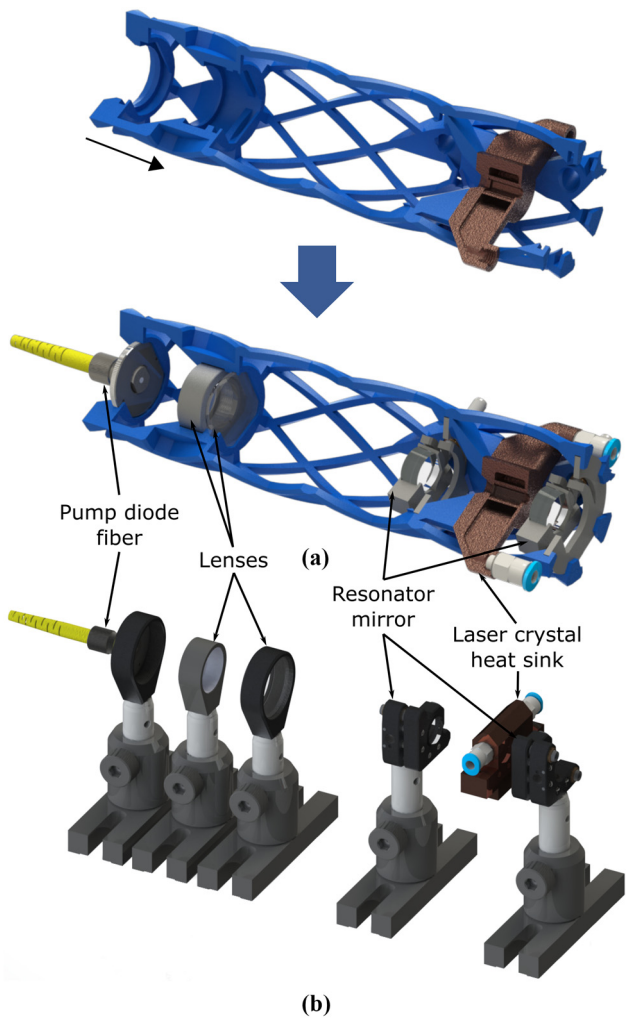

Source: Figure by authors

The laser system itself consists of a fiber-coupled pump diode with a 105 μm fiber core, a maximum output power of 8 W, and a central wavelength of 808 nm. The pump light was collimated and focused into the laser crystal with two lenses with focal lengths of 30 mm and 100 mm. The calculated beam waist diameter is approximately 380 μm. The laser crystal itself was a Nd:YVO_4-crystal with a doping concentration of 0.27 at.% and a length of 11 mm whereby the first 2 mm are undoped. Its position in the system is chosen so that the focal point of the pump light is in the center of the doped crystal section. The laser resonator consisted of a concave mirror with a radius of curvature of 1000 mm, a high-reflective coating at 1064 nm, and an anti-reflective coating at 808 nm. The output coupler was a plane mirror with a partial-reflective coating at 1064 nm of 90%. The distance between the first mirror and the laser crystal is 25 mm. A distance of 5 mm was chosen between the crystal and the second mirror. The distances as well as the lens configuration for the pump light were determined using optical simulations based on ABCD matrices.

5.2 Characterization

To quantify the functionality of the laser system with 3D printed optomechanics it was compared with a reference system built from discrete commercial optomechanics (cf. Figure 10(b)). Additionally, a copper-based heat sink was used in the reference setup. The evaluated parameters are listed below together with the respective measurement methods in the measurement setup shown in Figure 11:

- The maximum achievable laser output power is measured via *power head 1*.
- The long-term stability of the laser output power over a period of 8 h is also measured using *power head 1* and the percentage deviation over the measurement duration is determined.
- The optical-to-optical efficiency is calculated as the quotient between the maximum laser output power and the absorbed pump, using a *dichroic mirror* to separate the signal and pump light.
- The beam quality of the laser is defined by the beam quality parameter M^2. Measured with the *beam profile camera* according to the applicable standard (DIN11146-1, 2021).
- The beam position stability over time, called pointing, is measured via the *beam profile camera* over a period of 2 h.
- The power and thermal behavior of the system during repeated on- and off-cycles is determined.

Figure 11 Measurement setup used for verification of the laser system

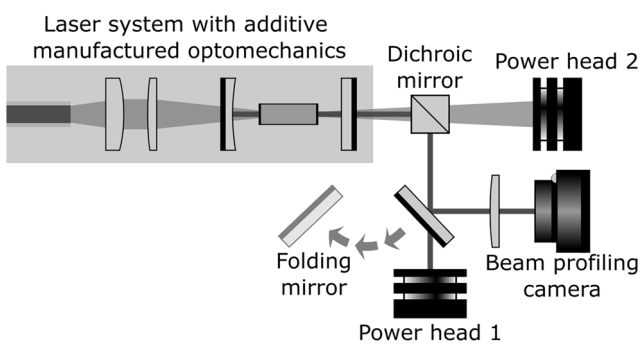

Source: Kranert, (2024)

A comparison of the results is presented in Table 7. In general, the laser output power and all the related parameters were higher in the reference system. At the same time, both the variation in the output power over time and the pointing are smaller. Only for the M^2-value the additive system shows a more convincing result. A reason for the improved characteristics of the reference system might be the improved thermal conductivity of the copper heat sink compared with that of the polymer material. Therefore, the cooling of the laser crystal is more efficient. Since the emission cross section inside a Nd:YVO_4-crystal is, among others, dependent on the temperature (Délen, *et al.*, 2011) the improved cooling can explain the higher output power of the reference system. Figure 12(a) shows the slope of the laser output power with respect to the absorbed pump power. A straight increase is visible, showing that the laser system's output power is limited by the available pump power and further scaling might be possible as long as the temperature limits of the used polymers are not reached. The long-term power stability is shown in Figure 12(b). It can be observed that the noise in the output power of the additive system is more pronounced. The thermal conductivities of the metallic and polymer-based heat sinks also influence the behavior of the two systems when they are switched on and off. Figure 13 shows the output power and temperature of the heat sinks for the two systems for several switching processes. It can be seen that, as expected, the heat dissipation of the metallic heat sink is higher and a thermal equilibrium is reached much faster, which means that the output power also reaches a stable level more quickly. However, it is also evident that both systems achieve their original output power even after multiple switching cycles, with no visible degradation.

As described, this characterization also aims to validate the design guidelines. The comparable laser operation output power between the reference and additive manufactured system demonstrates adequate precision and stability in placing and fixing these components within the matrix. Furthermore, the laser resonator, which utilizes printed adjustable optomechanics, and the evaluated ball joint demonstrated stable laser operation for several hours with a standard deviation of the optical output power of less than 1%. Similarly, the integrated and sealed water connections maintained a leak-free performance throughout the evaluation process. This highlights the effectiveness of the respective design guidelines.

Table 7 Overview of the parameters of the compared laser systems

Parameter	Reference system	Additive system
Max. output power / W	3.6	3.2
Slope efficiency / %	52.9 ± 0.3	51.1 ± 0.8
Standard deviation of the output power over 8 h / %	0.2	0.8
Optic-to-optical efficiency / %	50.4 ± 0.1	45.7 ± 0.4
M^2	1.42	1.32
Pointing RMS / µrad	1.9	19.9

Notes: Optical-to-optical efficiency and power stability are calculated and measured, respectively, at maximum output power. Same applies for the M^2. The accuracy of the power values is 3.0 % according to the specification of the power head. For the pointing, the beam position is detected over a period of 2 h

Source: Kranert, 2024

Figure 12 (a) Laser output power over absorbed pump power for both systems; (b) long-term measurement over 8 h of the output power and temperature of both systems' laser crystal's heat sinks

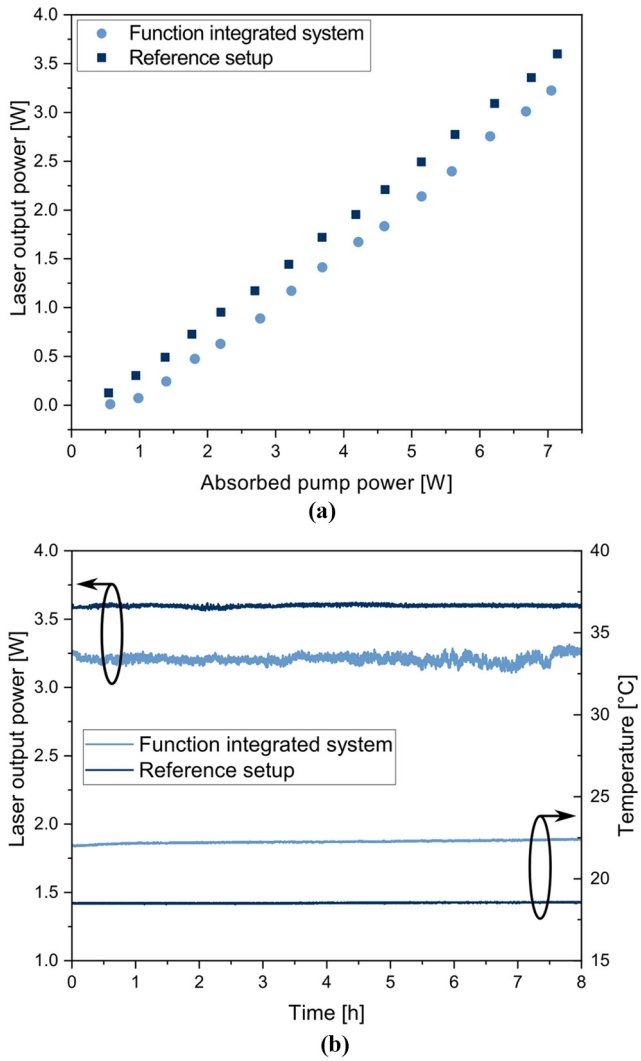

Source: Kranert, (2024)

6. Summary and conclusion

Additive manufacturing utilizing the FFF process has shown potential in various applications, including the production of optomechanical systems. However, the process's capacity for providing function-integrated systems is often not fully exploited. Function integration, though, offers great potential for achieving the goal of cost-efficient production set out in most studies addressing such applications, as a large number of technical functions can be implemented using a minimum number of components. For this reason, special attention is paid to the implementation of function integration. However, the development process of a DPSSL based on function-integrated optomechanics has revealed a possible obstacle, namely a deficiency in design guidelines that promote effective function integration. Based on the requirements elicited for the function-integrated optomechanics of a DPSSL, three key elements for function integration were identified (refer to Section 3). By a series of tests, conducted on suitable specimens, the

Figure 13 Measurement of laser output power and temperature at the heat sinks over several switching cycles

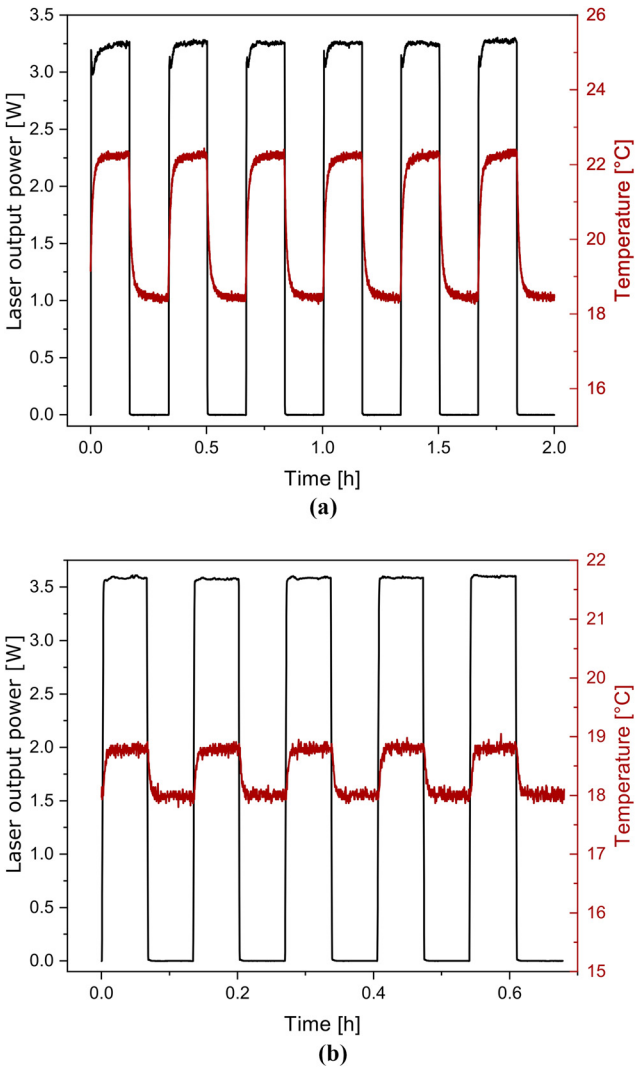

Notes: (a) System based on printed optomechanics; (b) reference system
Source: Kranert, (2024)

necessary design guidelines were formulated (refer to Table 6) and implemented into the design of the DPSSL:

- Optical elements must be integrated and mounted by imprinting within the optomechanics. The study uncovered the design parameters necessary for imprinting components, including stress-sensitive optics, into the polymer matrix of a printed component using the PpP process. The design guidelines enable a shift away from the discrete structure of optomechanical systems and significantly reduce the number of required components. The implementation of function integration as a design goal can be achieved by this. Adhering to the guidelines ensures a precise placement of components in the overall matrix, resulting in stable laser operation and validating the design guidelines.
- To ensure efficient cooling of the laser crystal, a water-cooling system is utilized. In order to increase function integration, the conditions under which watertight threads can be printed were investigated in an effort to eliminate the need for additional components. The study demonstrated that threads can be printed based on the formulated guidelines and that they are also long-term stable and tight in use.
- To achieve efficient laser operation, it is necessary to design resonator mirrors as adjustable optomechanics that include printed ball joints. The investigation examined the gap dimensions required for moving components with curved surfaces. Again, the characterization showed the successful implementation of the guidelines, allowing for further function integration.

Summing up, the highly sophisticated optomechanic for a DPSSL was printed and the intensive testing of the resulting laser system showed comparable results to a reference system based on conventional optomechanics. This proves the successful implementation of design guidelines, which can be easily adjusted for less demanding optomechanical systems. This means a diverse range of applications can benefit from the demonstrated options for compact and cost-effective systems. At the same time, the PpP process allows users without extensive experience in laser technology to implement the fabrication of laser systems, if the design of the optical system is known. Many areas, particularly those seeking cost savings, have the potential to benefit from this opportunity given the widespread use of lasers in research. Additionally, systems can be produced promptly on-site if the requisite optical components are accessible.

Previous research has identified a wealth of useful guidelines for the FFF process, which have been evaluated and confirmed in several studies. These guidelines allow users to design their components in a targeted and process-oriented manner even if they are inexperienced designers. These principles are extended by the derivations of the guidelines examined in this paper to further facilitate the production of systems with the design goal of function integration. In this way, the enormous potential of AM can be exploited even more effectively.

References

Adam, G. and Zimmer, D. (2014), "Design for additive manufacturing—element transitions and aggregated structures", *CIRP Journal of Manufacturing Science and Technology*, Vol. 7 No. 1, pp. 20-28, doi: 10.1016/j.cirpj.2013.10.001.

Adam, G. and Zimmer, D. (2015), "On design for additive manufacturing: evaluating geometrical limitations", *Rapid Prototyping Journal*, Vol. 21 No. 6, pp. 662-670, doi: 10.1108/rpj-06-2013-0060.

Alafaghani, A., Qattawi, A. and Ablat, M.A. (2017), "Design consideration for additive manufacturing: fused deposition modelling", *Open Journal of Applied Sciences*, Vol. 7 No. 6, pp. 291-318, doi: 10.4236/ojapps.2017.76024.

Aydogan, O. and Tasal, E. (2018), "Designing and building a 3D printed low cost modular Raman spectrometer", *CERN IdeaSquare Journal of Experimental Innovation*, Vol. 2 No. 2, pp. 3-14, doi: 10.23726/CIJ.2017.799.

Calignano, F., Manfredi, D., Ambrosio, E.P., Biamino, S., Lombardi, M., Atzeni, E., Salmi, A., Minetola, P., Iuliano, L. and Fino, P. (2017), "Overview on additive manufacturing technologies", *Proceedings of the IEEE*, Vol. 105 No. 4, pp. 593-612, doi: 10.1109/jproc.2016.2625098.

Davis, E.J., Jones, M., Thiel, D.A. and Pauls, S. (2018), "Using Open-Source, 3D printable optical hardware to enhance student learning in the instrumental analysis laboratory", *Journal of Chemical Education*, Vol. 95 No. 4, pp. 672-677, doi: 10.1021/acs.jchemed.7b00480.

Délen, X., Balembois, F. and Georges, P. (2011), "Temperature dependence of the emission cross section of Nd: YVO_4 around 1064nm and consequences on laser operation", *Journal of the Optical Society of America B*, Vol. 28 No. 5, pp. 972-976, doi: 10.1364/josab.28.000972.

Delmans, M. and Haseloff, J. (2018), "μCube: a framework for 3D printable optomechanics", *Journal of Open Hardware*, Vol. 2 No. 1, p. 2, doi: 10.5334/joh.8.

Diederich, B., Lachmann, R., Carlstedt, S., Marsikova, B. Wang, H., Uwurukundo, X., Mosig, A.S. and Heintzmann, R. (2020), "A versatile and customizable low-cost 3D-printed open standard for microscopic imaging", *Nature Communications*, Vol. 11 No. 1, p. 5979, doi: 10.1038/s41467-020-19447-9.

Diegel, O., (2022), "Design for AM", in Godec, D., Gonzalez-Gutierrez, J., Nordin, A., Pei, E. and Ureña Alcázar, J. (Eds), *A Guide to Additive Manufacturing*, Springer International Publishing, Cham, pp. 75-117, doi: 10.1007/978-3-031-05863-9_4.

Dilberoglu, U.M., Gharehpapagh, B., Yaman, U. and Dolen, M. (2017), "The role of additive manufacturing in the era of industry 4.0", *Procedia Manufacturing*, Vol. 11, pp. 545-554, doi: 10.1016/j.promfg.2017.07.148.

DIN11146-1 (2021), "DIN EN ISO 11146-1 - lasers and laser-related equipment - test methods for laser beam widths, divergence angles and beam propagation ratios - part 1: stigmatic and simple astigmatic beams", Beuth Verlag GmbH.

DIN336 (2003), "DIN 336 - diameters of drills for minor diameters of tapped threads", Beuth Verlag GmbH.

Djokikj, J. and Kandikjan, T. (2022), "DfAM: development of design rules for FFF", *Procedia CIRP*, Vol. 112, pp. 307-375, doi: 10.1016/j.procir.2022.09.011.

Elkholy, A., Rouby, M. and Kempers, R. (2019), "Characterization of the anisotropic thermal conductivity of additively manufactured components by fused filament fabrication", *Progress in Additive Manufacturing*, Vol. 4 No. 4, pp. 497-515, doi: 10.1007/s40964-019-00098-2.

Espalin, D., Ramirez, J.A., Medina, F. and Wicker, R. (2014), "Multi-material, multi-technology FDM: exploring build process variations", *Rapid Prototyping Journal*, Vol. 20 No. 3, pp. 236-244, doi: 10.1108/rpj-12-2012-0112.

Farniev, A., Novikov, P., Sidorov, D. and Falaleev, A. (2022), "Research of the accuracy of internal threads formed by FDM technology and additionally processed with tapers", *AIP Conference Proceedings*, Vol. 2503 No. 1, p. 70020, doi: 10.1063/5.0099407.

Gibson, I., Rosen, D.W. and Stucker, B. (2015), *Additive Manufacturing Technologies: 3D Printing, Rapid Prototyping and Direct Digital Manufacturing*, Springer, New York, NY, doi: 10.1007/978-1-4419-1120-9.

Gräßler, I., Hentze, J. and Bruckmann, T. (2018), "V-models for interdisciplinary systems engineering", in Marjanović, D., Štorga, M., Škec, S., Bojčetić, N. and Pavković, N. (Eds), DS 92: DESIGN 2018 15th International Design Conference, Faculty of Mechanical Engineering and Naval Architecture, University of Zagreb, *Zagreb*, pp. 747-756, doi: 10.21278/idc.2018.0333.

Gunderson, J.E., Mitchell, D.W., Bullis, R.G., Steward, J.Q. and Gunderson, W.A. (2020), "Design and implementation of Three-Dimensional printable optomechanical components", *Journal of Chemical Education*, Vol. 97 No. 10, pp. 3673-3682, doi: 10.1021/acs.jchemed.0c00631.

Haleem, A. and Javaid, M. (2019), "Additive manufacturing applications in industry 4.0: a review", *Journal of Industrial Integration and Management*, Vol. 04 No. 4, p. 1930001, doi: 10.1142/s2424862219300011.

Jordan, J. (2018), *3D Printing*, MIT Press, Cambridge.

Kerbrat, O., Mognol, P. and Hascoët, J.Y. (2011), "A new DFM approach to combine machining and additive manufacturing", *Computers in Industry*, Vol. 62 No. 7, pp. 684-692, doi: 10.1016/j.compind.2011.04.003.

Ko, H., Moon, S.K. and Hwang, J. (2015), "Design for additive manufacturing in customized products", *International Journal of Precision Engineering and Manufacturing*, Vol. 16 No. 11, pp. 2369-2375, doi: 10.1007/s12541-015-0305-9.

Koechner, W. (2006), *Solid-State Laser Engineering*, Springer, New York, NY.

Kranert, F., Budde, J., Hinkelmann, M., Neumann, J., Kracht, D. and Lachmayer, R. (2021a), "3D fabrication and characterization of polymer-imprinted optics for function-integrated, lightweight optomechanical systems", *Journal of Laser Applications*, Vol. 33 No. 4, p. 42010, doi: 10.2351/7.0000492.

Kranert, F., Budde, J., Hinkelmann, M., Neumann, J., Kracht, D. and Lachmayer, R. (2021b), "Thermische und strukturelle Analyse von Polymermaterialen in generativ gefertigten Optomechaniken für den Einsatz in der Laserentwicklung", *Clausthaler Zentrum Für Materialtechnik*, 4th ed.., Symposium Materialtechnik, Shaker, Düren, pp. 45-55.

Kranert, F., Budde, J., Hinkelmann, M., Lachmayer, R., Neumann, J. and Kracht, D. (2022),. "Additively manufactured polymer optomechanics and their application in laser systems", in Lachmayer, R., Kracht, D., Wesling, V. and Ahlers, H. (2022), "Additively manufactured polymer optomechanics and their application in laser systems", in Lachmayer, R., Kracht, D., Wesling, V. and Ahlers, H. (Eds), *Generative Manufacturing of Optical, Thermal and Structural Components (GROTESK)*, Springer International Publishing, Cham, pp. 25-50, doi: 10.1007/978-3-030-96501-3_2.

Kranert, F. (2024), "Potenziale der polymerbasierten additiven Fertigung für die Herstellung optomechanischer Systeme in der Laserentwicklung", PhD thesis, Gottfried Wilhelm Leibniz Universität Hannover.

Li, F., Macdonald, N.P., Guijt, R.M. and Breadmore, M.C. (2019), "Increasing the functionalities of 3D printed microchemical devices by single material, multimaterial, and print-pause-print 3D printing", *Lab on a Chip*, Vol. 19 No. 1, pp. 35-49, doi: 10.1039/c8lc00826d.

Maia Chagas, A., Prieto-Godino, L.L., Arrenberg, A.B. and Baden, T. (2017), "The €100 lab: a 3D-printable open-source platform for fluorescence microscopy, optogenetics, and accurate temperature control during behaviour of zebrafish, drosophila, and Caenorhabditis elegans", *PLoS Biology*, Vol. 15 No. 7, pp. 1-21, doi: 10.1371/journal.pbio.2002702.

Mani, M., Witherell, P. and Jee, H. (2017), "Design rules for additive manufacturing: a categorization", 37th Computers and

Information in Engineering Conference, *Cleveland*, American Society of Mechanical Engineers, doi: 10.1115/detc2017-68446.

Medellin-Castillo, H.I. and Zaragoza-Siqueiros, J. (2019), "Design and manufacturing strategies for fused deposition modelling in additive manufacturing: a review", *Chinese Journal of Mechanical Engineering*, Vol. 32 No. 1, doi: 10.1186/s10033-019-0368-0.

Nadal-Serrano, J.M., Nadal-Serrano, A. and Lopez-Vallejo, M. (2017), "Democratizing science with the aid of parametric design and additive manufacturing: design and fabrication of a versatile and low-cost optical instrument for scattering measurement", *PLoS One*, Vol. 12 No. 11, p. e0187219, doi: 10.1371/journal.pone.0187219.

Nefelov, I.S. and Baurova, N.I. (2017), "Formation of threaded surfaces in the components produced by 3D printing", *Russian Metallurgy (Metally)*, Vol. 2017 No. 13, pp. 1158-1160, doi: 10.1134/s0036029517130183.

Nuñez, I., Matute, T., Herrera, R., Keymer, J., Marzullo, T., Rudge, T. and Federici, F. (2017), "Low cost and open source multi-fluorescence imaging system for teaching and research in biology and bioengineering", *PloS One*, Vol. 12 No. 11, p. e0187163, doi: 10.1371/journal.pone.0187219.

Pearce, J.M. (2012), "Building research equipment with free, open-source hardware", *Science*, Vol. 337 No. 6100, pp. 1303-1304, doi: 10.1126/science.1228183.

Pereira, V.R. and Hosker, B.S. (2019), "Low-cost (<5€), open-source, potential alternative to commercial spectrophotometers", *PloS Biology*, Vol. 17 No. 6, p. e3000321, doi: 10.1371/journal.pbio.3000321.

Pinger, C.W., Heller, A.A. and Spence, D.M. (2017), "A printed equilibrium dialysis device with integrated membranes for improved binding affinity measurements", *Analytical Chemistry*, Vol. 89 No. 14, pp. 7302-7306, doi: 10.1021/acs.analchem.7b01848.

Porter, L.A., Chapman, C.A. and Alaniz, J.A. (2016), "Simple and inexpensive 3D printed filter fluorometer designs: user-Friendly instrument models for laboratory learning and outreach activities", *Journal of Chemical Education*, Vol. 94 No. 1, pp. 105-111, doi: 10.1021/acs.jchemed.6b00495.

Pradel, P., Zhu, Z., Bibb, R. and Moultrie, J. (2018), "A framework for mapping design for additive manufacturing knowledge for industrial and product design", *Journal of Engineering Design*, Vol. 29 No. 6, pp. 291-326, doi: 10.1080/09544828.2018.1483011.

Price, A.J.N., Capel, A.J., Lee, R.J., Pradel, P. and Christie, S. D.R. (2021), "An open source toolkit for 3D printed fluidics", *Journal of Flow Chemistry*, Vol. 11 No. 1, pp. 37-51, doi: 10.1007/s41981-020-00117-2.

Röttger, J., Grabe, T., Biermann, T., Ziebehl, A., Ley, P.-P., Wolf, A. and Lachmayer, R. (2021), "Multiphysical simulation approach for specifying material properties of additively manufactured laser heat sinks: potentials and challenges", *DGaO-Proceedings*, *Hannover*, doi: 10.15488/11521

Salazar-Serrano, L.J., Torres, J. and Valencia, A. (2017), "A 3D printed toolbox for Opto-Mechanical components", *PLoS One*, Vol. 12 No. 1, p. e0169832, doi: 10.1371/journal.pone.0169832.

Steuben, J., Van Bossuyt, D.L. and Turner, C. (2015), "Design for fused filament fabrication additive manufacturing", Proceedings of the ASME 2015 International Design Engineering Technical Conferences and Computers and Information in Engineering Conference. Volume 4: 20th Design for Manufacturing and the Life Cycle Conference; 9th International Conference on Micro- and Nanosystems, *Boston*, *American Society of Mechanical Engineers*, doi: 10.1115/detc2015-46355.

Thompson, M.K., Moroni, G., Vaneker, T., Fadel, G., Campbell, R.I., Gibson, I., Bernard, A., Schulz, J., Graf, P., Ahuja, B. and Martina, F. (2016), "Design for additive manufacturing: trends, opportunities, considerations, and constraints", *CIRP Annals*, Vol. 65 No. 2, pp. 737-760, doi: 10.1016/j.cirp.2016.05.004.

Urbanic, R.J. and Hedrick, R. (2016), "Fused deposition modeling design rules for building large, complex components", *Computer-Aided Design and Applications*, Vol. 13 No. 3, pp. 348-368, doi: 10.1080/16864360.2015.1114393.

VDI/VDE-Gesellschaft Mess-und Automatisierungstechnik (2021), VDI/VDE 2206: Development of mechatronic and cyber-physical systems", VDI/VDE standard.

VDI-Fachbereich Produktionstechnik und Verfahrenstechnik (2021), "VDI 3405 Sheet 3.4: Additive manufacturing processes – Design rules for part production using material extrusion processes", VDI standard, VDI-Gesellschaft Produktion und Logistik.

Winter, B. and Shepler, D. (2018), "3D printable optomechanical cage system with enclosure", *HardwareX*, Vol. 3, pp. 62-81, doi: 10.1016/j.ohx.2017.12.001.

Wynn, D., Caldwell, N. and Clarkson, P. (2010), "Can change prediction help prioritise redesign work in future engineering systems?", 11th International Design Conference DESIGN 2010, *Dubrovnik*, pp. 1691-1702.

Yang, S. and Zhao, Y. (2015), "Additive manufacturing-enabled design theory and methodology: a critical review", *The International Journal of Advanced Manufacturing Technology*, Vol. 80 , pp. 327-342, doi: 10.1007/s00170-015-6994-5.

Yoder, P. (2008), *Mounting Optics in Optical Instruments*, SPIE Press monograph, Bellingham.

Zhang, C., Anzalone, N.C., Faria, R.P. and Pearce, J.M. (2013), "Open-Source 3D-Printable optics equipment", *PLoS ONE*, Vol. 8 No. 3, p. e59840, doi: 10.1371/journal.pone.0059840.

Zou, L., Mahmoud, M., Fahs, M., Liu, R. and Lo, J.F. (2016), "3D printed miniaturized spectral system for tissue fluorescence lifetime measurements", in Farkas, D.L., Nicolau, D.V. and Leif, R.C. (Eds), *Imaging, Manipulation, and Analysis of Biomolecules, Cells, and Tissues IX*, SPIE, San Francisco, p. 97111S, doi: 10.1117/12.2217696.

Corresponding author

Fabian Kranert can be contacted at: f.kranert@lzh.de